crystals

MDPI

Article

An Overlooked Supramolecular Synthon in Multicomponent Trimethylglycine Crystals: Moderate Hydrogen Bonding Between Carboxylate and H-N Groups of Guanidine Species

Andrei V. Churakov [1], Alexander G. Medvedev [1], Nikita E. Frolov [2] and Mikhail V. Vener [1,*]

[1] N.S. Kurnakov Institute of General and Inorganic Chemistry, Russian Academy of Sciences, Leninskii Prosp. 31, Moscow 119991, Russia; churakov@igic.ras.ru (A.V.C.); mag@igic.ras.ru (A.G.M.)
[2] V. M. Gorbatov Federal Research Center for Food Systems, Talalikhina St. 26, Moscow 109316, Russia; frolovne24@gmail.com
* Correspondence: vener@igic.ras.ru

Abstract: Three novel multicomponent crystals of trimethylglycine with 2-cyanoguanidine, guanidinium and aminoguanidinium chlorides are synthesized and structurally characterized. All three crystal packings are based on the supramolecular synthon formed by two N–H groups of the guanidine species and carboxylate group of trimethylglycine (graph set notation $R^2_2(8)$). Its enthalpy is about 50 kJ/mol. The three-dimensional structure of crystals is stabilized by intermolecular interactions of various types. The energy of C–H···X^- interactions, where X = O, Cl, reaches 16 kJ/mol due to the acidic nature of methyl hydrogens. The possible structure of the trimethylglycine–urea–$2H_2O$ complex is discussed. Its theoretical metric and spectroscopic parameters are in reasonable agreement with the available literature data on the deep eutectic solvent trimethylglycine–urea.

Keywords: 2-cyanoguanidine; guanidinium cation; aminoguanidinium cation; N,N,N-trimethylglycine; periodic (solid-state) DFT computations; enthalpy of intermolecular hydrogen bonds; theoretical Raman spectra

Citation: Churakov, A.V.; Medvedev, A.G.; Frolov, N.E.; Vener, M.V. An Overlooked Supramolecular Synthon in Multicomponent Trimethylglycine Crystals: Moderate Hydrogen Bonding Between Carboxylate and H-N Groups of Guanidine Species. *Crystals* **2024**, *14*, 1050. https://doi.org/10.3390/cryst14121050

Academic Editor: Jesús Sanmartín-Matalobos

Received: 14 October 2024
Revised: 24 November 2024
Accepted: 28 November 2024
Published: 30 November 2024

1. Introduction

Much attention is paid to the creation of single- and multi-component crystals with functional properties [1,2], in particular, pharmaceutical two-component crystals [3–5]. In such studies, the concept of supramolecular synthon is widely used [6–9]. Different types of these synthons exist in multicomponent crystals and are caused by intermolecular hydrogen bonds (H-bonds), see Figure 4 in [10]. The energy of these H-bonds has been estimated [11,12]. Of particular note are the supramolecular synthons formed between acids and aminopyrimidines, 2-aminopyridines, etc. [13–15]. Such synthons are very suitable for the creation of multicomponent crystals of active pharmaceutical ingredients (APIs) [13] and can play a role in fine-tuning their solubility [16]. Depending on the strength of the base, ionic or neutral synthons can be formed (Scheme 2 in [13]). This makes it difficult to predict which of the two supramolecular synthons is formed in any given case.

Trimethylglycine (betaine, TMG) plays an important role in the metabolism of plants, animals and humans [17,18]. It is now widely used as a component of pharmaceuticals and dietary supplements [19,20]. TMG is a zwitterion in gas and condensed phases. In the absence of strong monobasic acids [21], it forms H-bonds via the carboxylate group. This simplifies the process of creation of multi-component API crystals. Different types of synthons formed by the carboxylate group of TMG with hydroxyl groups were studied in [22]. The resulting strong intermolecular bonds O–H···O^- form a variety of supramolecular heterosynthons, in particular, a nine-membered cycle with two O–H···O^- bonds between L-ascorbic acid and TMG zwitterion, which can be described by graph set notation $R^2_2(9)$ [23]. The Cambridge Structural Database [24] contains the structures of various multi-component

crystals of TMG with polybasic inorganic acids. For example, in crystalline TMG–arsenate (Table S1), there is a heterosynthon with two short O–H···O$^-$ bonds (graph set notation $R^2_2(8)$). Much less attention has been paid to the creation of multi-component crystals in which the carboxylate group of TMG interacts with the coformer molecule via N–H···O bonds. Such bonds are realized in the urea–TMG inclusion compound [25]. The distance between the "heavy" atoms of the N–H···O fragment is around 3.0 Å, and comparable to those in crystalline urea [26].

TMG is a co-crystal former used to improve the tabletability of paracetamol [27], the solubility of flavonoids [28], etc. [29,30]. Due to its biological and pharmaceutical applications [31–33], TMG is a promising compound for obtaining highly soluble co-crystals of the "drug-drug" or "API-API" type [34,35]. In this paper, we considered guanidine species as APIs, since they are a group of arginine metabolites [36]. A number of in vitro and animal studies have shown that guanidines exert pro-inflammatory effects on monocyte and macrophage function [37]. Potential areas of application of TMG crystals with guanidine compounds are both the creation of highly soluble API–API crystals and their use in natural deep eutectic solvents (NADESs) based on TMG [38].

In the present study, three multicomponent crystals of TMG with guanidine species were synthesized and structurally characterized (Scheme 1). Periodic (solid-state) DFT calculations allow us to identify and quantify intermolecular interactions in these crystals. The results of this study, in conjunction with our previous paper devoted to aqueous complexes of TMG [39], allowed us to create a NADES structure consisting of TMG, urea and water with a molar ratio of components (1:1:2) under non-anhydrous conditions.

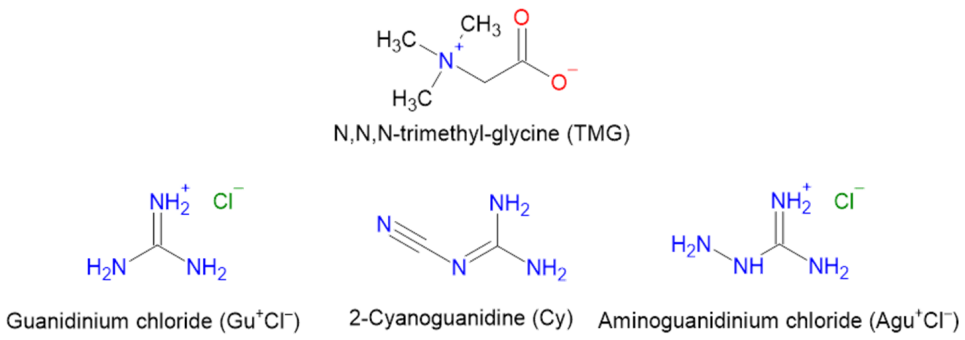

Scheme 1. Molecular structures of TMG and the studied guanidine species.

2. Materials and Methods

2.1. Synthesis

Betaine anhydrous (97%) was obtained from TCI Chemicals (Tokyo, Japan), 2-cyanoguanidine (98.5%) and guanidinium chloride (99.5%) were purchased from Chemcraft (Kaliningrad, Russia), and aminoguanidinium chloride (98%) and methanol (99%) were purchased from Thermo Fisher Scientific (Waltham, MA, USA). [TMG•Gu$^+$Cl$^-$] (2:1) was prepared by dissolving TMG (0.2342 g, 2 mmol) and guanidinium chloride (0.0955 g, 1 mmol) in 10 mL of methanol. The solution was slowly evaporated until colorless crystals precipitated at room temperature. The crystalline powder was filtered and dried in a vacuum desiccator for 30 min. [TMG•Cy] (1:1) was prepared by dissolving TMG (0.1171 g, 1 mmol) and 2-cyanoguanidine (0.0841 g, 1 mmol) in 5 mL of methanol. The colorless crystals were obtained by slow evaporation of the solvent at room temperature. The crystalline powder was filtered and dried in a vacuum desiccator for 30 min. [TMG•Agu$^+$Cl$^-$] (2:1) was prepared by dissolving TMG (0.2342 g, 2 mmol) and aminoguanidinium chloride (0.1105 g, 1 mmol) in 5 mL of methanol. The colorless crystals were obtained by slow evaporation of the solvent at room temperature. The crystalline powder was filtered and dried in a vacuum desiccator for 30 min.

2.2. Single-Crystal XRD

Single crystals of [TMG•Gu+Cl^-], [TMG•Cy] and [TMG•Agu+Cl^-] suitable for X-ray diffraction analysis were collected from the corresponding mother liquor without additional recrystallization. Single-crystal diffraction data were collected using a Bruker D8 Venture diffractometer (Bruker AXS, Bremen, Germany) with graphite-monochromated Cu-K_α radiation (λ = 1.54178 Å) for 2-cyanoguanidine [TMG•Cy] and [TMG•Gu+Cl^-] and a Bruker SMART Photon II machine (Mo-K_α radiation, λ = 0.71073 Å) for [TMG•Agu+Cl^-]. Absorption corrections based on measurements of equivalent reflections were applied [40]. The structures were solved by direct methods and refined using full matrix least-squares on F^2 with anisotropic thermal parameters for all non-hydrogen atoms [41]. All hydrogen atoms were found with difference Fourier synthesis and refined isotropically. Experimental details are listed in Table S2. The crystallographic data were deposited with the Cambridge Crystallographic Data Centre as supplementary publications under the CCDC numbers 2381711-2381713. This information can be obtained free of charge from the Cambridge Crystallographic Data Centre via www.ccdc.cam.ac.uk/data_request/cif, accessed on 18 July 2024.

2.3. Computational Details

2.3.1. Periodic DFT Computations

PBE [42] and B3LYP functionals [43,44] were used in the present study. The consistent introduction of dispersion corrections into the B3LYP method is not straightforward [45,46]. Therefore, the D3 correction [47] was only taken into account in the PBE calculations. PBE-D3 and B3LYP are successfully used in calculating various properties of multi-component crystals [48–54]. The atoms were described with a 6-31G** basis set. Computations were conducted using CRYSTAL17 [55]. When optimizing the crystal structure, experimental values of the space group and unit cell parameters were used [56], known as the "AtomOnly" option [55]. Computation details are given in the Supplementary Materials.

2.3.2. The Enthalpy of H-Bonds and the Energy of Intermolecular Interactions

Unlike molecular complexes in vacuum, the quantitative characterization of non-covalent interactions and intermolecular H-bonds in crystals is not unambiguous. The exceptions are a few crystals in which the enthalpy of sublimation is determined by some type of non-covalent interaction or H-bond, with typical examples being CF_4 [57,58] and water ices [59,60]. For a number of intermolecular interactions of a certain type and strength, empirical approaches have been proposed that allow one to estimate the enthalpy or energy of the interaction from metric [61] or electro-topological parameters [62]. The values of these parameters can be found with experiments or calculated using periodic (solid-state) DFT methods. It should be noted that the works [61,62] consider precisely intermolecular H-bonds in molecular complexes and crystals.

In this study, it was assumed that a non-covalent (intermolecular) interaction and H-bond is realized when there is a point (3,-1) on the bond path [63] between the atoms of neighboring molecules in a crystal. Bader's analysis of the crystal electron density was conducted using Topond 14 [64].

The enthalpy of H-bond ΔH_{HB} in kJ/mol was estimated using [61]

$$-\Delta H_{HB} = 0.134 \cdot R(H \cdots O)^{-3.05}, \quad (1)$$

R(H···O) denotes the distance H···O in nm. Its values were computed using PBE-D3 and B3LYP.

The energy of non-covalent interaction E_{int} in kJ/mol was estimated using [62]

$$E_{int} = 0.429 \cdot G_b, \quad (2)$$

G_b denotes the local electronic kinetic energy density at the bond critical point [63].

3. Results

In the present work, three crystals of TMG with guanidinium chloride [TMG•Gu+Cl^-] (2:1), 2-Cyanoguanidine [TMG•Cy] (1:1), and aminoguanidinium chloride [TMG•Agu+Cl^-] (2:1) were obtained and structurally characterized (see Table S1, Figures S1–S5). The details, results and discussion of phase characterization using powder XRD and thermal analysis are given in the Supporting Information file (Materials and Methods section, Figures S6–S12).

The asymmetric unit in the structure [TMG•Gu+Cl^-] (2:1) consists of two crystallographically independent TMG molecules, one guanidine cation and one chloride anion (Figure S1). In crystal, these components are combined in almost planar centrosymmetric insular motif (Figure S2) via N–H···^-O_2C– and N–H···Cl^- moderate H-bonds. It should be noted that the guanidine cation is linked to both TMG zwitterions via two almost linear H-bonds due to the successful geometric complementarity of the carboxyl and guanidine fragments. The structure [TMG•Agu+Cl^-] (2:1), as previously mentioned [TMG•Gu+Cl^-] (2:1), comprises two independent TMG molecules, one aminoguanidine cation and one chloride anion (Figure S5). In crystal, all building units are combined in chains passing along the *a*-axis via N–H···^-O_2C– and N–H···Cl^- interactions. The structure [TMG•Cy] (1:1) consists of one independent TMG zwitterion and one cyanoguanidine molecule (Figure S3). In crystal, adjacent molecules are linked in the chains parallel to the *c*-axis via N–H···O and N–H···N bonds. In contrast to the [TMG•Gu+Cl^-] (2:1) structure, guanidine moieties serve as both the donor and acceptor of H-bonds (Figure S4). In all three structures, bond lengths and angles adopt ordinary values for TMG and guanidine derivatives. All active N*H* hydrogen atoms are involved in hydrogen bonding.

The three crystals contain a supramolecular heterosynthon built by two N–H groups of the guanidine derivative and TMG carboxylate group of $R^2_2(8)$ topology. The heterodimeric $R^2_2(8)$ synthon between guanidinium and carboxylate ions is the building block in organic crystals [65–67]. The orientation of molecules in the synthon is determined by lateral H-bonds and is coplanar in [TMG•Gu+Cl^-] (2:1) and [GB•Agu+Cl^-] (2:1) and twisted in [TMG•Cy] (1:1). In ternary crystals, guanidine derivatives do not form H-bonds with each other. The guanidine derivatives form five "unique" intermolecular H-bonds with three adjacent TMG molecules and an H-bond with the chlorine ion (Figures 1 and 2).

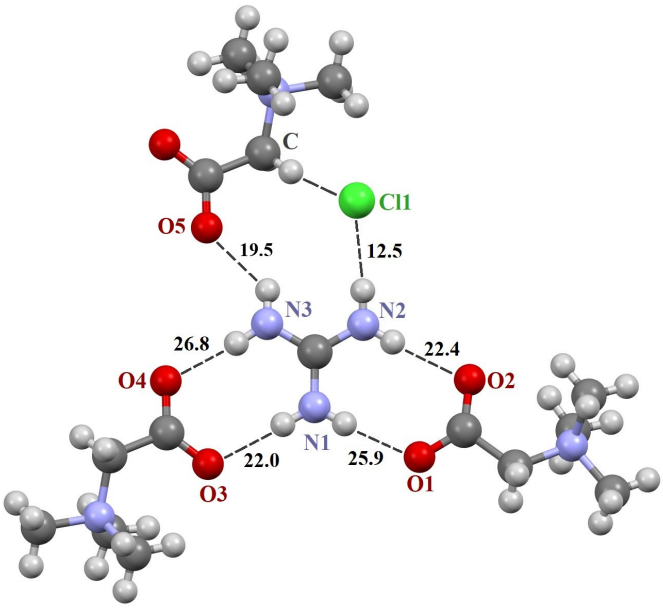

Figure 1. Fragments of crystal structures [TMG•Gu+Cl^-] (2:1). Unique H-bonds are drawn as dashed lines. Numbers indicate the H-bond enthalpies (kJ/mol) evaluated using Equation (1) at the B3LYP level.

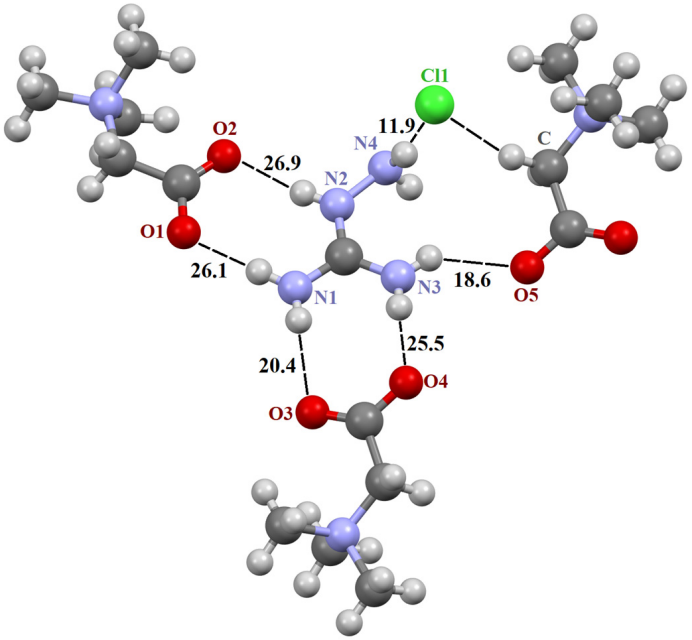

Figure 2. Fragment of crystal structure [TMG•Agu+Cl^-] (2:1). Unique H-bonds are drawn as dashed lines. Numbers indicate the H-bond enthalpies (kJ/mol) evaluated using Equation (1) at the B3LYP level.

The N–H···O^- bonds forming two $R^2_2(8)$ synthons are almost linear, with the N···O distance varying from 2.794 to 2.983 Å (Table 1), in agreement with the literature data [3,66,68,69]. The fifth N–H···O^- bond is formed with the third TMG molecule, which lies in the plane formed by two $R^2_2(8)$ synthons. This H-bond is highly nonlinear (Table 1). The sixth N–H group interacts with the chlorine ion. This anion locates well below the plane and interacts with four C–H groups of the three TMG molecules that locate in the different planes.

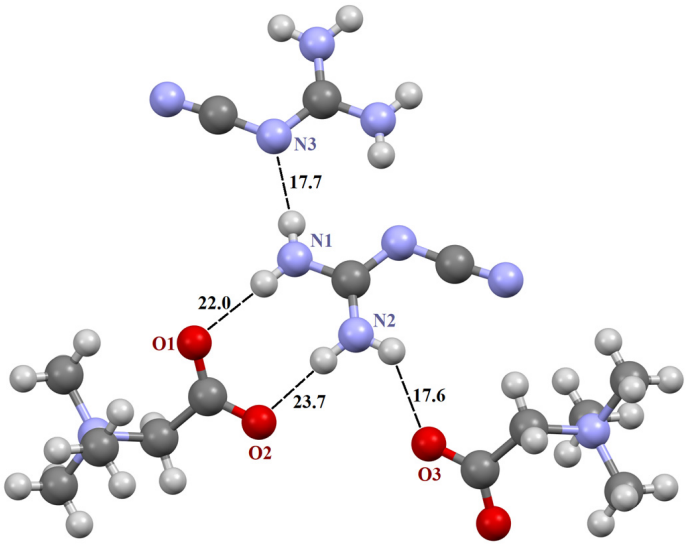

Figure 3. Fragment of crystal structure [TMG•Cy] (1:1). Unique H-bonds are drawn as dashed lines. Numbers indicate the H-bond enthalpies (kJ/mol) evaluated using Equation (1) at the B3LYP level.

Table 1. Experimental values of metric parameters of H-bonded fragments in the three crystals: distance between heavy atoms R(X···Y), R_{exp}, and fragment angle X–H···Y (Angle), where X = N, C and Y = O, Cl, N.

Fragment [a]	[TMG•Gu+Cl⁻] (2:1)		[TMG•Agu+Cl⁻] (2:1)		[TMG•Cy] (1:1)	
	R_{exp}, Å	Angle, deg.	R_{exp}, Å	Angle, deg.	R_{exp}, Å	Angle, deg.
N1–H···O1	2.818	173.4	2.798	176.6	2.912	177.7
N2–H···O2	2.887	172.1	2.801	173.9	2.863	169.4
N1–H···O3	2.900	175.8	2.983	165.1	-	-
N3–H···O4	2.794	175.2	2.807	174.7	-	-
N3–H···O5	2.862	136.6	2.893	141.9	-	-
N2–H···Cl1	3.218	163.3	-	-	-	-
N4–H···Cl1	-	-	3.290	166.6	-	-
N1–H···N3	-	-	-	-	3.010	172.7
N2–H···O3	-	-	-	-	2.853	135.0
C–H···Cl1	3.621	159.3	3.598	162.4	-	-

[a] atomic numeration is given in Figures 1–3.

2-cyanoguanidine forms four "unique" intermolecular hydrogen bonds with three neighboring molecules: two TMG and one 2-cyanoguanidine (Figure 3). As a result of the interaction of guanidine derivatives in this two-component crystal, a $R^2_2(8)$ synthon with two N–H...N bonds arises.

The hydrogen bond enthalpy ΔH_{HB} of the three crystals, calculated using Equation (1), is given in Table 2. The total enthalpy of the $R^2_2(8)$ synthon formed by two N–H groups of the guanidine derivative and the TMG carboxylate group (46–53 kJ/mol) is practically independent of the nature of the guanidine derivative. The obtained ΔH_{HB} values are consistent with the literature data [70]. The total enthalpy of the $R^2_2(8)$ synthon with two N–H...N bonds equals to 35 kJ/mol. This value is consistent with the literature data [71–73].

Table 2. The difference between the computed and experimental value of the distance between heavy atoms ΔR [a] of unique H-bonds in the three crystals. The H-bond enthalpy ΔH_{HB} (kJ/mol) was estimated using Equation (1). The values calculated at the PBE-D3 level are given in italics.

Fragment [b]	[TMG•Gu+Cl⁻] (2:1)		[TMG•Agu+Cl⁻] (2:1)		[TMG•Cy] (1:1)	
	ΔR, Å	$-\Delta H_{HB}$	ΔR, Å	$-\Delta H_{HB}$	ΔR, Å	$-\Delta H_{HB}$
N1–H···O1	0.01	25.9	−0.011	26.1	0.014	22.0
	0.017	*26.8*	- [c]	-	*0.016*	*22.4*
N2–H···O2	−0.003	22.4	0.012	26.9	0.011	23.7
	0.017	*23.7*	-	-	*0.027*	*24.8*
N1–H···O3	−0.002	22.0	0.053	20.4	-	-
	−0.003	*22.4*	-	-		
N3–H···O4	0.004	26.8	−0.009	25.5	-	-
	−0.011	*28.0*	-	-		
N3–H···O5 [d]	0.046	19.5	0.030	18.6	-	-
	0.056	*20.0*	-	-		
N2–H···Cl1	−0.039	12.5	-	-	-	-
	−0.026	*13.1*				
N4–H···Cl1	-	-	−0.023	11.9	-	-
			-	-		
N1–H···N3	-	-	-	-	−0.020	17.7
					−0.001	*18.5*
N2–H···O3 [c]	-	-	-	-	0.001	17.6
					0.011	*18.2*

[a] $\Delta R = R_{exp} - R_{calc}$, R_{exp} values are given in Table 1; [b] atomic numeration is given in Figures 1–3; [c] PBE-D3 calculations yielded one imaginary frequency (10 cm^{-1}) for this crystal; therefore, the enthalpy values computed in this approximation are not given in the table; [d] this H-bond is highly nonlinear (see Table 1).

The B3LYP and PBE-D3 levels give similar metric parameters of H-bonded fragments in the three crystals and, therefore, close values of enthalpies of H-bonds (Table 2). Comparison of Table 2 and Table S3 shows that Equations (1) and (2) lead to similar values of ΔH_{HB} and E_{int}. This is due to the fact that relatively weak hydrogen bonds [74] exist in the crystals under consideration [75].

In all crystals, TMG zwitterions interact with each other via C–H··· O^- bonds. Their energy, estimated using Equation (2), is about 13 kJ/mol, which is consistent with the literature data [39,76]. The energy of some C–H···O^- bonds can reach 16 kJ/mol. This is due to the acidic nature of the hydrogens of the methylene and methyl groups.

In the crystals under consideration, a large number of different non-covalent interactions are also realized. The most common are the C···N, C–H···N, H···H, and C–H···Cl^- interactions. Their energy, estimated by Equation (2), usually does not exceed ~6 kJ/mol. However, the energy of some interactions turns out to be higher than this value. In particular, C–H···Cl^- interactions occur with an energy of about 10 kJ/mol. The obtained energies are consistent with literature data [77].

In recent years, Raman spectroscopy has been widely used in the study of polymorphism of molecular crystals [51], including APIs [78], H-bonds and non-covalent interactions in single- [79] and multi-component [56,80,81] molecular crystals, etc. [52]. A discussion of the theoretical Raman spectra of the three crystals is given in the Supplementary Materials.

4. Discussion

Recently, much attention has been paid to the development of NADES [82,83], which is composed, in particular, of urea, TMG and guanidine species [38,84,85]. The nature of the intermolecular interactions between NADES components has been investigated, e.g., see [86,87]; however, most studies have focused on the macroscopic properties of NADES. The results of the present study, in conjunction with our previous paper devoted to aqueous complexes of TMG [39], have allowed us to create a NADES structure consisting of TMG, urea and water with a molar ratio of components (1:1:2) [38]. This complex will be further designated as TMG–urea–$2H_2O$.

The structure of TMG with two water molecules is shown in Figure 1 [39]. It corresponds to the global minimum, and the total enthalpy of intermolecular hydrogen bonds in it is about 100 kJ/mol (Scheme 1 in [39]). From the results of the present study, it follows that the N–H groups of urea will form a heterosynthon with two N–H···O^- bonds with the carboxylate group of TMG (graph set notation $R^2_2(8)$). Geometry optimization of the TMG–urea–$2H_2O$ complex was performed using the B3LYP/6-31G** approximation. The structure of this complex is shown in Figure 5 [39]. The total enthalpy of intermolecular H-bonds in the TMG–urea–$2H_2O$ complex is about 138 kJ/mol. Obviously, it will be quite stable in non-aqueous conditions. In contrast, the solvate-separated TMG–urea complexes discussed in [87] should be treated as short-lived species [88].

To verify the created structure of the TMG–urea–$2H_2O$ complex, its metric and spectral parameters were compared with available literary data (details of non-periodic computations and Cartesian coordinates of the complex are given in the Supplementary Materials). The distance between the TMG oxygen and the water oxygen of the O2–H···O1 fragment (Figure 4) is 2.75 Å, which is consistent with the value of 2.67 Å obtained in the molecular dynamics simulations of TMG–urea mixtures [86]. The calculated IR spectrum of the complex contains three bands lying in the range of 1700–1450 cm^{-1}, which is consistent with the data presented in Figure 5 of Ref. [87]. According to our computations, the band at about 1600 cm^{-1} is associated with bending vibrations of two water molecules. The calculated values of chemical shifts of hydrogen atoms $\delta(^1H)$ of the complex are compared with the available literature data in Table 3. The agreement is satisfactory.

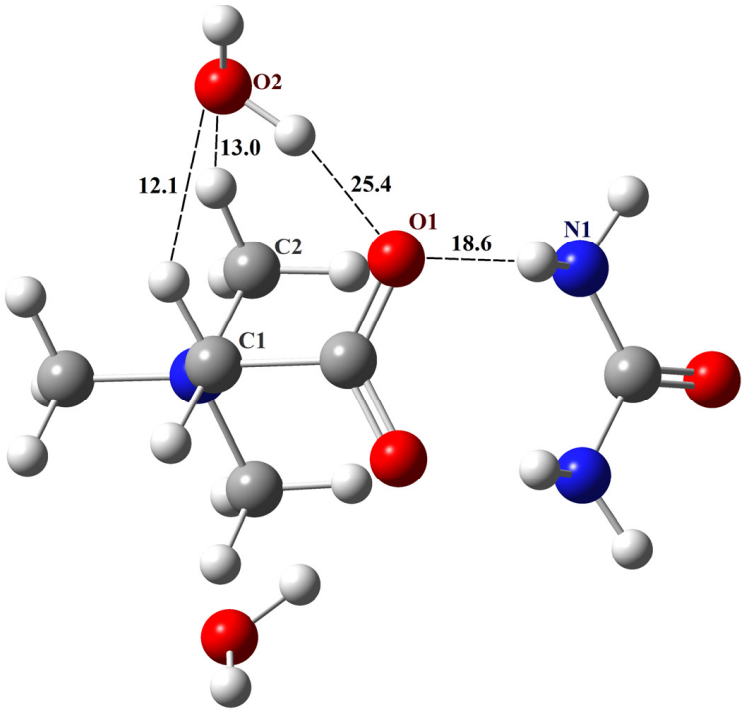

Figure 4. The structure of the TMG–urea–$2H_2O$ complex. Unique H-bonds are drawn as dashed lines. Numbers indicate the H-bond enthalpies (kJ/mol) evaluated using Equation (1) at the B3LYP level.

Table 3. Comparison of the calculated values of $\delta(^1H)$ of the TMG–urea–$2H_2O$ complex compared with the available literature data (Figure 4A1 of Ref. [87]).

This Study		[87]	
$\delta(^1H)$, ppm	**Assignment**	**$\delta(^1H)$, ppm**	**Assignment**
6.58	H-bonded OH	-	-
6.36	H-bonded NH	5.94	NH_2
4.56, 4.24, 4.14	H-bonded CH of CH_3 and CH_2 groups	4.54	H_2O
3.01, 2.86	"free" NH and CH of CH_3 groups	3.00	CH_3

5. Conclusions

Three novel multicomponent crystals of N,N,N-trimethyl-glycine (TMG) with guanidinium chloride [TMG•Gu+Cl^-] (2:1), 2-cyanoguanidine [TMG•Cy] (1:1), and aminoguanidinium chloride [TMG•Agu+Cl^-] (2:1) were synthesized and structurally characterized. All three crystal packings are based on a synthon formed by two N–H groups of the guanidine derivative and the carboxylate group of TMG (graph set notation $R^2_2(8)$). The N–H···O^- bonds forming $R^2_2(8)$ synthons are almost linear, with the N···O distance varying from 2.794 to 2.983 Å. Crystalline [TMG•Cy] (1:1) is an example of the $R^2_2(8)$ synthon with N–H···O^- bonds between the neutral molecule and TMG.

Intermolecular interactions in three crystals are identified and quantified using periodic DFT calculations. The total enthalpy of the $R^2_2(8)$ synthon formed by two N–H groups of the guanidine derivative and the TMG carboxylate group (46–53 kJ/mol) is practically independent of the nature of the guanidine derivative. As a result of the interaction of guanidine derivatives in the [TMG•Cy] (1:1) crystal, the $R^2_2(8)$ synthon with two N–H...N bonds arises. Its enthalpy equals 35 kJ/mol. The three-dimensional structure of crystals is stabilized by C–H···X^- interactions, where X = O, Cl. Their energy reaches 10 and 16 kJ/mol, respectively, due to the acidic nature of methyl hydrogens.

Supplementary Materials: The following supporting information can be downloaded at: https://www.mdpi.com/article/10.3390/cryst14121050/s1, Table S1: Multicomponent TMG crystals grouped by heterosynthon type, Table S2: Crystallographic data, details of the SC-XRD experiment and structure refinement for multicomponent crystals of N,N,N-trimethyl-glycine with guanidine derivatives obtained in this study, Table S3: The difference between the computed and experimental value of the distance between heavy atoms ΔR of unique H-bonds in the three crystals. The H-bond energy E_{int} (kJ/mol) was evaluated using Equation (2). The values calculated at the PBE-D3 level are given in italics, Table S4: Wavenumbers (cm^{-1}) of the Raman-active vibrations of the three crystals in the low-frequency region calculated using solid-state DFT in the B3LYP/6-31G** and PBE-D3/6-31G** approximations., Table S5: Wavenumbers (cm^{-1}) of the Raman-active modes of three crystals in the high-frequency region calculated using solid-state DFT in the B3LYP/6-31G** and PBE-D3/6-31G** approximations, Figure S1: Asymmetric unit in the structure [TMG•Gu+Cl^-] (2:1). Thermal ellipsoids are shown at 50% probability level. Hydrogen bonds are drawn as dashed lines, Figure S2: Hydrogen bonded insular motif in the structure [TMG•Gu+Cl^-] (2:1), Figure S3: Asymmetric unit in the structure [TMG•Cy] (1:1). Thermal ellipsoids are shown at 50% probability level. Hydrogen bonds are drawn as dashed lines, Figure S4: Hydrogen bonded chains along c-axis in the structure [TMG•Cy] (1:1), Figure S5: Asymmetric unit in the structure [TMG•Agu+Cl^-] (2:1). Thermal ellipsoids are shown at 50% probability level. Hydrogen bonds are drawn as dashed lines, Figure S6: Comparison of theoretical (a) and experimental (b) X-ray powder diffractograms of [TMG•Gu+Cl^-] (2:1), Figure S7: Comparison of theoretical (a) and experimental (b) X-ray powder diffractograms of [TMG•Cy] (1:1), Figure S8: Comparison of theoretical (a) and experimental (b) X-ray powder diffractograms of [TMG•Agu+Cl^-] (2:1), Figure S9: The thermal analysis of [TMG•Gu+Cl^-] (2:1): weight loss (blue) and DTA signal (red), Figure S10: The thermal analysis of [TMG•Cy] (1:1): weight loss (blue) and DTA signal (red), Figure S11: The DSC cycling curves of [TMG•Cy] (1:1), Figure S12: The thermal analysis of [TMG•Agu+Cl^-] (2:1): weight loss (blue) and DTA signal (red), Figure S13: Displacements of atoms of the most intense mode in three crystals (solid-state DFT calculations using the B3LYP/6-31G** approximation), Cartesian coordinates (Å) of the TMG–urea–2H2O complex, Video file TMG_Cy.avi confirming the assumption about the phase transition and subsequent melting [TMG•Cy] (1:1).

Author Contributions: Conceptualization, A.V.C. and M.V.V.; experimental methodology, A.V.C. and A.G.M.; theoretical methodology, M.V.V.; investigation, A.G.M., A.V.C. and N.E.F.; single-crystal XRD experiment, A.V.C.; writing—original draft preparation, N.E.F. and M.V.V.; writing—review and editing, A.G.M. and M.V.V.; visualization, N.E.F.; supervision, M.V.V. and A.V.C. All authors have read and agreed to the published version of the manuscript.

Funding: This work was supported by the Ministry of Science and Higher Education of the Russian Federation, as part of the State Assignment of the Kurnakov Institute of General and Inorganic Chemistry RAS.

Data Availability Statement: Crystal structures of [TMG•Gu+Cl^-] (2:1), [TMG•Cy] (1:1) and [TMG•Agu+Cl^-] (2:1) have been deposited with the Cambridge Crystallographic Data Centre, under the CCDC numbers 2381711-2381713.

Acknowledgments: M.V.V. thanks Oleg G. Kharlanov (Lomonosov Moscow State University) for the useful discussions of low-frequency Raman spectra and German L. Perlovich (Institute of Solution Chemistry RAS, Ivanovo) for the possibility of conducting computations using Crystal17. X-ray diffraction studies were performed using the equipment of the JRC PMR IGIC RAS.

Conflicts of Interest: The authors declare no conflicts of interest.

References

1. Bellas, M.K.; Matzger, A.J. Peroxosolvate Discovery Method Leads to First Cocrystal with Three Energetic Components. *Chem. Commun.* **2022**, *58*, 8806–8809. [CrossRef] [PubMed]
2. Jaime-Adán, E.; Hernández-Ortega, S.; Toscano, R.A.; Germán-Acacio, J.M.; Sánchez-Pacheco, A.D.; Hernández-Vergara, M.; Barquera, J.E.; Valdés-Martínez, J. Competition of Hydrogen Bonds, Halogen Bonds, and π–π Interactions in Crystal Structures. Exploring the Effect of One Atom Substitution. *Cryst. Growth Des.* **2024**, *24*, 1888–1897. [CrossRef]
3. Babu, N.J.; Reddy, L.S.; Nangia, A. Amide−*N*-Oxide Heterosynthon and Amide Dimer Homosynthon in Cocrystals of Carboxamide Drugs and Pyridine *N*-Oxides. *Mol. Pharm.* **2007**, *4*, 417–434. [CrossRef] [PubMed]

4. Li, N.; Chen, Y.; Chen, R.; Zhang, M.; Wu, T.; Liu, K. Synthesis and Structure Characterization of Three Pharmaceutical Compounds Based on Tinidazole. *Crystals* **2023**, *13*, 947. [CrossRef]
5. Voronin, A.P.; Ramazanova, A.G.; Churakov, A.V.; Vologzhanina, A.V.; Kulikova, E.S.; Perlovich, G.L. Virtual Screening, Polymorphism, and Formation Thermodynamics Study of Riluzole Multicomponent Crystals with Dihydroxybenzoic Acids. *Cryst. Growth Des* **2024**. [CrossRef]
6. Desiraju, G.R. Crystal Engineering: From Molecule to Crystal. *J. Am. Chem. Soc.* **2013**, *135*, 9952–9967. [CrossRef]
7. Shishkin, O.V.; Zubatyuk, R.I.; Shishkina, S.V.; Dyakonenko, V.V.; Medviediev, V.V. Role of Supramolecular Synthons in the Formation of the Supramolecular Architecture of Molecular Crystals Revisited from an Energetic Viewpoint. *Phys. Chem. Chem. Phys.* **2014**, *16*, 6773. [CrossRef]
8. Mukherjee, A.; Desiraju, G.R. Combinatorial Exploration of the Structural Landscape of Acid–Pyridine Cocrystals. *Cryst. Growth Des.* **2014**, *14*, 1375–1385. [CrossRef]
9. Mukherjee, A. Building upon Supramolecular Synthons: Some Aspects of Crystal Engineering. *Cryst. Growth Des.* **2015**, *15*, 3076–3085. [CrossRef]
10. Deng, Y.; Liu, S.; Jiang, Y.; Martins, I.C.B.; Rades, T. Recent Advances in Co-Former Screening and Formation Prediction of Multicomponent Solid Forms of Low Molecular Weight Drugs. *Pharmaceutics* **2023**, *15*, 2174. [CrossRef]
11. Dunitz, J.D.; Gavezzotti, A. Supramolecular Synthons: Validation and Ranking of Intermolecular Interaction Energies. *Cryst. Growth Des.* **2012**, *12*, 5873–5877. [CrossRef]
12. Vener, M.V.; Levina, E.O.; Koloskov, O.A.; Rykounov, A.A.; Voronin, A.P.; Tsirelson, V.G. Evaluation of the Lattice Energy of the Two-Component Molecular Crystals Using Solid-State Density Functional Theory. *Cryst. Growth Des.* **2014**, *14*, 4997–5003. [CrossRef]
13. Bis, J.A.; Zaworotko, M.J. The 2-Aminopyridinium-Carboxylate Supramolecular Heterosynthon: A Robust Motif for Generation of Multiple-Component Crystals. *Cryst. Growth Des.* **2005**, *5*, 1169–1179. [CrossRef]
14. Ebenezer, S.; Muthiah, P.T. Design of Co-Crystals/Salts of Aminopyrimidines and Carboxylic Acids through Recurrently Occurring Synthons. *Cryst. Growth Des.* **2012**, *12*, 3766–3785. [CrossRef]
15. Garg, U.; Azim, Y.; Kar, A.; Pradeep, C.P. Cocrystals/Salt of 1-Naphthaleneacetic Acid and Utilizing Hirshfeld Surface Calculations for Acid–Aminopyrimidine Synthons. *CrystEngComm* **2020**, *22*, 2978–2989. [CrossRef]
16. da Silva, C.C.; Cirqueira, M.d.L.; Martins, F.T. Lamivudine Salts with 1,2-Dicarboxylic Acids: A New and a Rare Synthon with Double Pairing Motif Fine-Tuning Their Solubility. *CrystEngComm* **2013**, *15*, 6311. [CrossRef]
17. Holm, P.I.; Bleie, Ø.; Ueland, P.M.; Lien, E.A.; Refsum, H.; Nordrehaug, J.E.; Nygaård, O. Betaine as a Determinant of Postmethionine Load Total Plasma Homocysteine Before and After B-Vitamin Supplementation. *Arterioscler. Thromb. Vasc. Biol.* **2004**, *24*, 301–307. [CrossRef]
18. Schwab, U.; Törrönen, A.; Toppinen, L.; Alfthan, G.; Saarinen, M.; Aro, A.; Uusitupa, M. Betaine Supplementation Decreases Plasma Homocysteine Concentrations but Does Not Affect Body Weight, Body Composition, or Resting Energy Expenditure in Human Subjects. *Am. J. Clin. Nutr.* **2002**, *76*, 961–967. [CrossRef]
19. Mäkelä, P. Agro-Industrial Uses of Glycinebetaine. *Sugar Tech.* **2004**, *6*, 207–212. [CrossRef]
20. Turck, D.; Castenmiller, J.; De Henauw, S.; Hirsch-Ernst, K.I.; Kearney, J.; Maciuk, A.; Mangelsdorf, I.; McArdle, H.J.; Naska, A.; Pelaez, C.; et al. Safety of Betaine as a Novel Food Pursuant to Regulation (EU) 2015/2283. *EFSA J.* **2019**, *17*, e05658. [CrossRef]
21. Godzisz, D.; Ilczyszyn, M.M.; Ilczyszyn, M. Classification and Nature of Hydrogen Bonds to Betaine. X-Ray, 13 C CP MAS and IR Description of Low Barrier Hydrogen Bonds. *J. Mol. Struct.* **2002**, *606*, 123–137. [CrossRef]
22. Kavuru, P.; Aboarayes, D.; Arora, K.K.; Clarke, H.D.; Kennedy, A.; Marshall, L.; Ong, T.T.; Perman, J.; Pujari, T.; Wojtas, Ł.; et al. Hierarchy of Supramolecular Synthons: Persistent Hydrogen Bonds between Carboxylates and Weakly Acidic Hydroxyl Moieties in Cocrystals of Zwitterions. *Cryst. Growth Des.* **2010**, *10*, 3568. [CrossRef]
23. Etter, M.C. Encoding and Decoding Hydrogen-Bond Patterns of Organic Compounds. *Acc. Chem. Res.* **1990**, *23*, 120–126. [CrossRef]
24. Groom, C.R.; Bruno, I.J.; Lightfoot, M.P.; Ward, S.C. The Cambridge Structural Database. *Acta Crystallogr. B Struct. Sci. Cryst. Eng. Mater* **2016**, *72*, 171–179. [CrossRef]
25. Yang, Y.; Lu, Z. Novel Urea/Thiourea-Betaine Inclusion Compounds Consolidated by Host-Guest Hydrogen Bonds. *Mol. Cryst. Liq. Cryst.* **2021**, *722*, 47–57. [CrossRef]
26. Swaminathan, S.; Craven, B.M.; McMullan, R.K. The Crystal Structure and Molecular Thermal Motion of Urea at 12, 60 and 123 K from Neutron Diffraction. *Acta Crystallogr. Sect. B* **1984**, *40*, 300–306. [CrossRef]
27. Maeno, Y.; Fukami, T.; Kawahata, M.; Yamaguchi, K.; Tagami, T.; Ozeki, T.; Suzuki, T.; Tomono, K. Novel Pharmaceutical Cocrystal Consisting of Paracetamol and Trimethylglycine, a New Promising Cocrystal Former. *Int. J. Pharm.* **2014**, *473*, 179–186. [CrossRef]
28. Zhang, Z.; Li, D.; Luo, C.; Huang, C.; Qiu, R.; Deng, Z.; Zhang, H. Cocrystals of Natural Products: Improving the Dissolution Performance of Flavonoids Using Betaine. *Cryst. Growth Des.* **2019**, *19*, 3851–3859. [CrossRef]
29. Kamal, G.; Abdullah, S.; Basingab, F.; Bani-Jaber, A.; Hamdan, I.I. Curcumin-Betaine Solid Dispersion for Enhancing Curcumin Dissolution and Potentiating Pharmacological Synergism in Gastric Cancer Cells. *J. Drug Deliv. Sci. Technol.* **2023**, *79*, 103951. [CrossRef]

30. Oliveira, P.V.; Aguiar, G.P.S.; Siebel, A.M.; Müller, L.G.; Lerin, L.A.; Botti, G.; Bianchi, A.; Bernardi, T.; Gentili, V.; Rizzo, R.; et al. Synthesis of Naringenin-Betaine Cocrystal by Gas Antisolvent Technique and Cell Models for in Vitro Permeation Studies. *J. Drug Deliv. Sci. Technol.* **2024**, *96*, 105671. [CrossRef]
31. Ashraf, M.; Foolad, M.R. Roles of Glycine Betaine and Proline in Improving Plant Abiotic Stress Resistance. *Environ. Exp. Bot.* **2007**, *59*, 206–216. [CrossRef]
32. Figueroa-Soto, C.G.; Valenzuela-Soto, E.M. Glycine Betaine Rather than Acting Only as an Osmolyte Also Plays a Role as Regulator in Cellular Metabolism. *Biochimie* **2018**, *147*, 89–97. [CrossRef]
33. Dobrijević, D.; Pastor, K.; Nastić, N.; Özogul, F.; Krulj, J.; Kokić, B.; Bartkiene, E.; Rocha, J.M.; Kojić, J. Betaine as a Functional Ingredient: Metabolism, Health-Promoting Attributes, Food Sources, Applications and Analysis Methods. *Molecules* **2023**, *28*, 4824. [CrossRef] [PubMed]
34. Port, A.; Almansa, C.; Enrech, R.; Bordas, M.; Plata-Salamán, C.R. Differential Solution Behavior of the New API-API Co-Crystal of Tramadol-Celecoxib (CTC) versus Its Constituents and Their Combination. *Cryst. Growth Des.* **2019**, *19*, 3172–3182. [CrossRef]
35. Perlovich, G.L. Two-Component Molecular Crystals: What Is the Difference between Drug-Drug, Drug-GRAS, and CF-CF Databases? Evaluation of Melting Points and Ideal Solubility of Unknown Co-Crystals. *Cryst. Growth Des.* **2021**, *21*, 5058–5071. [CrossRef]
36. Rosner, M.H.; Husain-Syed, F.; Reis, T.; Ronco, C.; Vanholder, R. Uremic Encephalopathy. *Kidney Int.* **2022**, *101*, 227–241. [CrossRef]
37. Devetzis, V.; Zarogoulidis, P.; Kakolyris, S.; Vargemezis, V.; Chatzaki, E. The Corticotropin Releasing Factor System in the Kidney: Perspectives for Novel Therapeutic Intervention in Nephrology. *Med. Res. Rev.* **2013**, *33*, 847–872. [CrossRef]
38. Cvjetko Bubalo, M.; Andreou, T.; Panić, M.; Radović, M.; Radošević, K.; Radojčić Redovniković, I. Natural Multi-Osmolyte Cocktails Form Deep Eutectic Systems of Unprecedented Complexity: Discovery, Affordances and Perspectives. *Green Chem.* **2023**, *25*, 3398–3417. [CrossRef]
39. Frolov, N.E.; Shishkina, A.V.; Vener, M.V. Specific Proton-Donor Properties of Glycine Betaine. Metric Parameters and Enthalpy of Noncovalent Interactions in Its Dimer, Water Complexes and Crystalline Hydrate. *Int. J. Mol. Sci.* **2023**, *24*, 12971. [CrossRef]
40. Sheldrick, G. SADABS, Program for Scaling and Correction of Area Detector Data. University of Gottingen: Göttingen, Germany, 1996.
41. Sheldrick, G.M. A Short History of SHELX. *Acta Crystallogr. A* **2008**, *64*, 112–122. [CrossRef]
42. Perdew, J.P.; Burke, K.; Ernzerhof, M. Generalized Gradient Approximation Made Simple. *Phys. Rev. Lett.* **1996**, *77*, 3865. [CrossRef] [PubMed]
43. Becke, A.D. Density-Functional Thermochemistry. III. The Role of Exact Exchange. *J. Chem. Phys.* **1993**, *98*, 2155–2160. [CrossRef]
44. Lee, C.; Yang, W.; Parr, R.G. Development of the Colle-Salvetti Correlation-Energy Formula into a Functional of the Electron Density. *Phys. Rev. B* **1988**, *37*, 785. [CrossRef] [PubMed]
45. Goerigk, L.; Grimme, S. A Thorough Benchmark of Density Functional Methods for General Main Group Thermochemistry, Kinetics, and Noncovalent Interactions. *Phys. Chem. Chem. Phys.* **2011**, *13*, 6670. [CrossRef]
46. Merten, C. Modelling Solute–Solvent Interactions in VCD Spectra Analysis with the Micro-Solvation Approach. *Phys. Chem. Chem. Phys.* **2023**, *25*, 29404–29414. [CrossRef]
47. Grimme, S.; Ehrlich, S.; Goerigk, L. Effect of the Damping Function in Dispersion Corrected Density Functional Theory. *J. Comput. Chem.* **2011**, *32*, 1456–1465. [CrossRef]
48. Mohaček-Grošev, V.; Grdadolnik, J.; Stare, J.; Hadži, D. Identification of Hydrogen Bond Modes in Polarized Raman Spectra of Single Crystals of α-Oxalic Acid Dihydrate. *J. Raman Spectrosc.* **2009**, *40*, 1605–1614. [CrossRef]
49. Yushina, I.D.; Kolesov, B.A.; Bartashevich, E.V. Raman Spectroscopy Study of New Thia- and Oxazinoquinolinium Triodides. *New J. Chem.* **2015**, *39*, 6163–6170. [CrossRef]
50. Cutini, M.; Civalleri, B.; Corno, M.; Orlando, R.; Brandenburg, J.G.; Maschio, L.; Ugliengo, P. Assessment of Different Quantum Mechanical Methods for the Prediction of Structure and Cohesive Energy of Molecular Crystals. *J. Chem. Theory Comput.* **2016**, *12*, 3340–3352. [CrossRef]
51. Bedoya-Martínez, N.; Schrode, B.; Jones, A.O.F.; Salzillo, T.; Ruzié, C.; Demitri, N.; Geerts, Y.H.; Venuti, E.; Della Valle, R.G.; Zojer, E.; et al. DFT-Assisted Polymorph Identification from Lattice Raman Fingerprinting. *J. Phys. Chem. Lett.* **2017**, *8*, 3690–3695. [CrossRef]
52. Vener, M.V.; Kharlanov, O.G.; Sosorev, A.Y. High-Mobility Naphthalene Diimide Derivatives Revealed by Raman-Based In Silico Screening. *Int. J. Mol. Sci.* **2022**, *23*, 13305. [CrossRef]
53. Rogers, F.J.M.; Radhanpura, K.; Horvat, J.; Farrant, D. On the Use of a Volume Constraint to Account for Thermal Expansion Effects on the Low-Frequency Vibrations of Molecular Crystals. *Phys. Chem. Chem. Phys.* **2022**, *24*, 10405–10419. [CrossRef]
54. Beērziņš, K.; Sutton, J.J.; Fraser-Miller, S.J.; Rades, T.; Korter, T.M.; Gordon, K.C. Solving the Computational Puzzle: Toward a Pragmatic Pathway for Modeling Low-Energy Vibrational Modes of Pharmaceutical Crystals. *Cryst. Growth Des.* **2020**, *20*, 6947–6955. [CrossRef]
55. Dovesi, R.; Erba, A.; Orlando, R.; Zicovich-Wilson, C.M.; Civalleri, B.; Maschio, L.; Rérat, M.; Casassa, S.; Baima, J.; Salustro, S.; et al. Quantum-Mechanical Condensed Matter Simulations with CRYSTAL. *Wiley Interdiscip. Rev. Comput. Mol. Sci.* **2018**, *8*, e1360. [CrossRef]

56. Voronin, A.P.; Surov, A.O.; Churakov, A.V.; Parashchuk, O.D.; Rykounov, A.A.; Vener, M.V. Combined X-Ray Crystallographic, IR/Raman Spectroscopic, and Periodic DFT Investigations of New Multicomponent Crystalline Forms of Anthelmintic Drugs: A Case Study of Carbendazim Maleate. *Molecules* **2020**, *25*, 2386. [CrossRef]
57. Chickos, J.S.; Gavezzotti, A. Sublimation Enthalpies of Organic Compounds: A Very Large Database with a Match to Crystal Structure Determinations and a Comparison with Lattice Energies. *Cryst. Growth Des.* **2019**, *19*, 6566–6576. [CrossRef]
58. Levina, E.O.; Chernyshov, I.Y.; Voronin, A.P.; Alekseiko, L.N.; Stash, A.I.; Vener, M.V. Solving the Enigma of Weak Fluorine Contacts in the Solid State: A Periodic DFT Study of Fluorinated Organic Crystals. *RSC Adv.* **2019**, *9*, 12520–12537. [CrossRef]
59. Ruckenstein, E.; Shulgin, I.L.; Shulgin, L.I. Cooperativity in Ordinary Ice and Breaking of Hydrogen Bonds. *J. Phys. Chem. B* **2007**, *111*, 7114–7121. [CrossRef]
60. Vener, M.V.; Egorova, A.N.; Tsirelson, V.G. Hydrogen Bonds and O$\cdots$O Interactions in Proton-Ordered Ices. DFT Computations with Periodic Boundary Conditions. *Chem. Phys. Lett.* **2010**, *500*, 272–276. [CrossRef]
61. Rozenberg, M.; Loewenschuss, A.; Marcus, Y. An Empirical Correlation between Stretching Vibration Redshift and Hydrogen Bond Length. *Phys. Chem. Chem. Phys.* **2000**, *2*, 2699–2702. [CrossRef]
62. Mata, I.; Alkorta, I.; Espinosa, E.; Molins, E. Relationships between Interaction Energy, Intermolecular Distance and Electron Density Properties in Hydrogen Bonded Complexes under External Electric Fields. *Chem. Phys. Lett.* **2011**, *507*, 185–189. [CrossRef]
63. Bader, R.F.W. A Quantum Theory of Molecular Structure and Its Applications. *Chem. Rev.* **1991**, *91*, 893–928. [CrossRef]
64. Gatti, C.; Cassasa, S. *TOPOND14 User's Manual*; CNR-ISTM of Milano: Milano, Italy, 2013.
65. Yadav, V.N.; Görbitz, C.H. A Supramolecular 2:1 Guanidinium-Carboxylate Based Building Block for Generation of Water Channels and Clusters in Organic Materials. *CrystEngComm* **2013**, *15*, 439–442. [CrossRef]
66. Adachi, T.; Ward, M.D. Versatile and Resilient Hydrogen-Bonded Host Frameworks. *Acc. Chem. Res.* **2016**, *49*, 2669–2679. [CrossRef]
67. Dillon, A.M.; Yusov, A.; Chaudhry, M.T.; Newman, J.A.; Demkiw, K.M.; Woerpel, K.A.; Lee, A.Y.; Ward, M.D. Supramolecular Mille-Feuille: Adaptive Guest Inclusion in a New Aliphatic Guanidinium Monosulfonate Hydrogen-Bonded Framework. *Cryst. Growth Des.* **2024**, *24*, 3483–3490. [CrossRef]
68. Oruganti, M.; Khade, P.; Das, U.K.; Trivedi, D.R. The Hierarchies of Hydrogen Bonds in Salts/Cocrystals of Isoniazid and Its Schiff Base—A Case Study. *RSC Adv.* **2016**, *6*, 15868–15876. [CrossRef]
69. Yadav, B.; Balasubramanian, S.; Chavan, R.B.; Thipparaboina, R.; Naidu, V.G.M.; Shastri, N.R. Hepatoprotective Cocrystals and Salts of Riluzole: Prediction, Synthesis, Solid State Characterization, and Evaluation. *Cryst. Growth Des.* **2018**, *18*, 1047–1061. [CrossRef]
70. Surov, A.O.; Vasilev, N.A.; Churakov, A.V.; Parashchuk, O.D.; Artobolevskii, S.V.; Alatortsev, O.A.; Makhrov, D.E.; Vener, M.V. Two Faces of Water in the Formation and Stabilization of Multicomponent Crystals of Zwitterionic Drug-like Compounds. *Symmetry* **2021**, *13*, 425. [CrossRef]
71. Tupikina, E.Y.; Sigalov, M.; Shenderovich, I.G.; Mulloyarova, V.V.; Denisov, G.S.; Tolstoy, P.M. Correlations of NHN Hydrogen Bond Energy with Geometry and 1 H NMR Chemical Shift Difference of NH Protons for Aniline Complexes. *J. Chem. Phys.* **2019**, *150*, 114305. [CrossRef]
72. Voronin, A.P.; Perlovich, G.L.; Vener, M.V. Effects of the Crystal Structure and Thermodynamic Stability on Solubility of Bioactive Compounds: DFT Study of Isoniazid Cocrystals. *Comput. Theor. Chem.* **2016**, *1092*, 1–11. [CrossRef]
73. Mirzaei, M.; Sadeghi, F.; Molčanov, K.; Zaręba, J.K.; Gomila, R.M.; Frontera, A. Recurrent Supramolecular Motifs in a Series of Acid–Base Adducts Based on Pyridine-2,5-Dicarboxylic Acid *N* -Oxide and Organic Bases: Inter- and Intramolecular Hydrogen Bonding. *Cryst. Growth Des.* **2020**, *20*, 1738–1751. [CrossRef]
74. Steiner, T. The Hydrogen Bond in the Solid State. *Angew. Chem. Int. Ed.* **2002**, *41*, 48–76. [CrossRef]
75. Medvedev, A.G.; Churakov, A.V.; Navasardyan, M.A.; Prikhodchenko, P.V.; Lev, O.; Vener, M.V. Fast Quantum Approach for Evaluating the Energy of Non-Covalent Interactions in Molecular Crystals: The Case Study of Intermolecular H-Bonds in Crystalline Peroxosolvates. *Molecules* **2022**, *27*, 4082. [CrossRef]
76. Voronin, A.P.; Volkova, T.V.; Ilyukhin, A.B.; Trofimova, T.P.; Perlovich, G.L. Structural and Energetic Aspects of Adamantane and Memantine Derivatives of Sulfonamide Molecular Crystals: Experimental and Theoretical Characterisation. *CrystEngComm* **2018**, *20*, 6680. [CrossRef]
77. Serebryanskaya, T.V.; Novikov, A.S.; Gushchin, P.V.; Haukka, M.; Asfin, R.E.; Tolstoy, P.M.; Kukushkin, V.Y. Identification and H(D)-bond energies of C–H(D)...Cl interactions in chloride–haloalkane clusters: A combined X-ray crystallographic, spectroscopic, and theoretical study. *Phys. Chem. Chem. Phys.* **2016**, *18*, 14104–14112. [CrossRef]
78. Kendrick, J.; Burnett, A.D. Exploring the Stability and Disorder in the Polymorphs of L-Cysteine through Density Functional Theory and Vibrational Spectroscopy. *Cryst. Growth Des.* **2023**, *23*, 5734–5747. [CrossRef]
79. Takahashi, M. Terahertz Vibrations and Hydrogen-Bonded Networks in Crystals. *Crystals* **2014**, *4*, 74–103. [CrossRef]
80. Surov, A.O.; Vasilev, N.A.; Vener, M.V.; Parashchuk, O.D.; Churakov, A.V.; Magdysyuk, O.V.; Perlovich, G.L. Pharmaceutical Salts of Fenbendazole with Organic Counterions: Structural Analysis and Solubility Performance. *Cryst. Growth Des.* **2021**, *21*, 4516–4530. [CrossRef]
81. Song, M.; Yang, F.; Su, C.; Deng, B. Characterizing Hydrogen Bonds in Crystalline Form of Guanidinium Salicylate in the Terahertz Range. *RSC Adv.* **2020**, *11*, 307–319. [CrossRef]

82. Tian, Y.; Sun, D.-W.; Zhu, Z. Development of Natural Deep Eutectic Solvents (NADESs) as Anti-Freezing Agents for the Frozen Food Industry: Water-Tailoring Effects, Anti-Freezing Mechanisms and Applications. *Food Chem.* **2022**, *371*, 131150. [CrossRef]
83. Wawoczny, A.; Gillner, D. The Most Potent Natural Pharmaceuticals, Cosmetics, and Food Ingredients Isolated from Plants with Deep Eutectic Solvents. *J. Agric. Food Chem.* **2023**, *71*, 10877–10900. [CrossRef] [PubMed]
84. Dai, Y.; van Spronsen, J.; Witkamp, G.-J.; Verpoorte, R.; Choi, Y.H. Natural Deep Eutectic Solvents as New Potential Media for Green Technology. *Anal. Chim. Acta* **2013**, *766*, 61–68. [CrossRef] [PubMed]
85. Olivares, B.; Martínez, F.; Rivas, L.; Calderón, C.; Munita, J.M.; Campodonico, P.R. A Natural Deep Eutectic Solvent Formulated to Stabilize β-Lactam Antibiotics. *Sci. Rep.* **2018**, *8*, 14900. [CrossRef] [PubMed]
86. Kumar, N.; Kishore, N. Synergistic Behavior of Glycine Betaine-Urea Mixture: A Molecular Dynamics Study. *J. Chem. Phys.* **2013**, *139*, 115104. [CrossRef]
87. Nava-Ocampo, M.F.; Al Fuhaid, L.; Santana, A.; Bucs, S.S.; Verpoorte, R.; Hae Choi, Y.; Witkamp, G.J.; Vrouwenvelder, J.S.; Farinha, A.S.F. Structural Properties and Stability of the Betaine-Urea Natural Deep Eutectic Solvent. *J. Mol. Liq.* **2021**, *343*, 117655. [CrossRef]
88. Vener, M.V.; Odinokov, A.V.; Wehmeyer, C.; Sebastiani, D. The Structure and IR Signatures of the Arginine-Glutamate Salt Bridge. Insights from the Classical MD Simulations. *J. Chem. Phys.* **2015**, *142*, 215166. [CrossRef]